Particle Acceleration in the Presence of Weak Turbulence at an X-Type Neutral Point

C.A. Burge[1,3], P. Petkaki[2], and A.L. MacKinnon[1]

[1]SUPA School of Physics & Astronomy, University of Glasgow, G12 8QQ, UK email: c.burge@astro.gla.ac.uk, alexander.mackinnon@glasgow.ac.uk
[2] DAMTP, Centre for Mathematical Sciences, University of Cambridge, CB3 0WA, UK email: P.Petkaki@damtp.cam.ac.uk
[3] British Antarctic Survey, Cambridge, CB3 0ET, UK

April 2, 2012

Abstract

We simulate the likely noisy situation near a reconnection region by superposing many 2D linear reconnection eigenmodes. The superposition of modes on the steady state X-type magnetic field creates multiple X- and O-type neutral points close to the original neutral point and so increases the size of the non-adiabatic region. We study test particle trajectories of initially thermal protons in these fields. Protons become trapped in this region and are accelerated by the turbulent electric field to energies up to 1 MeV in time scales relevant to solar flares. Higher energies are achieved due to the interaction of particles with increasingly turbulent electric and magnetic fields.

1 Introduction

Transient, intense radiation across the electromagnetic spectrum bears witness to the acceleration of particles to high energies in astrophysical plasmas. Solar flares give a particularly well-studied example, with their impulsive phase hard X-ray, γ-ray and radio signatures *e.g.* Lin *et al.* (2003); White

1

et al. (2011).The high energies of the emitting particles appear to be consequences of magnetic reconnection, in which energy is released rapidly from the non-potential component of the magnetic field via a change in field line connectivity *e.g.* Priest and Forbes (2000). The physical processes by which this can happen remain unclear.

As yet, no model exists which accounts for all of the observed properties of the energy release in solar flares. Early reconnection models *e.g.* Sweet (1958); Parker (1963) considered the resistive structure of steady current sheets and the resulting reconnection rate. However, these models gave reconnection rates that were much too slow to produce plasma outflows at the observed speeds. Petschek (1964) suggested that higher outflow speeds can be reached if a central region dominated by wave propagation is introduced.

Bulanov and Syrovatskii (1980) were the first to propose that such waves could be magnetohydrodynamic (MHD) in nature, and considered an X-type neutral point perturbed by harmonic fast waves that are azimuthally symmetric. An X-type neutral point is a type of magnetic field which contains a central point at which the magnetic field goes to zero and which is divided into four regions of different connectivity, divided by separatrices. At the centre of the region, (*i.e.* at the neutral point) particles decouple from the magnetic field and are freely accelerated by any electric field present (*i.e.* in this region the particle moves non-adiabatically). Such magnetic field configurations are therefore often considered when modelling reconnection regions in the solar corona.

Bulanov and Syrovatskii (1980) considered a two-dimensional (2D) cylindrically symmetric geometry, and perturbed the system at r=1 (the system boundary). They found that these perturbations became azimuthally symmetric as they approached the null. Initially, this symmetry meant that it was unclear if this result was applicable more generally. However, Craig and co-authors ((Craig and McClymont, 1991),1993,Craig and Watson (1992)) found that reconnection can only occur if the wave modes perturbing the neutral point have azimuthal symmetry.

The simplicity of the X-type neutral point field and the associated description of linear reconnection provide a prototypical picture in which particle acceleration may be studied. Petkaki and MacKinnon (1997),(2007) considered an X-type neutral point being perturbed by single eigenmode oscillations, similar to those studied in Craig and McClymont's work, and found that this oscillation increased the efficiency of the neutral point as a particle accelerator. This was shown to be due to the finite width of the non-adiabatic region close to the neutral point which allows particles to gain or lose energy randomly resulting in a Fermi-type stochastic acceleration. Furthermore Petkaki and MacKinnon (2007),2011 found that certain frequencies

were more effective at accelerating particles than others, through resonant interactions, since some particles were observed to gain energy outside of the central diffusion region (see also Guo *et al.* (2010) and the analytical discussion of Litvinenko (2003)).

This work seeks to extend these models by examining the effects of weak turbulence on the reconnection region and on particle behaviour. This turbulence will be introduced by considering a superposition of MHD eigenmodes. It is likely that a viable solution to the problem must be time dependent. This is because steady state solutions cannot adequately deal with the large-scale advection of the plasma as well as the small-scale diffusion region around the neutral point. The motivation for introducing this time dependence via a time-dependent electric field comes from the idea of linear reconnection as stated by Craig and McClymont (1991). The structure and evolution of the reconnection region imply the form of the electric field which we use to accelerate particles in our simulations.

2   Electric and Magnetic Fields

Following Craig and McClymont (1991) and Petkaki and MacKinnon (1997) we study the behaviour of test particles in a system with translational invariance in the z-direction. Then the magnetic field may be written:

$$\mathbf{B} = \nabla \times (\psi(x, y, t)\hat{\mathbf{z}}) \tag{1}$$

$\mathbf{B}$ and the associated velocity field $\mathbf{V}$ will be calculated in a cold plasma model. The electric field then follows from Equation 1 via Ohm's law. We write:

$$\psi(x, y, t) \;=\; \psi_0(x, y) + \frac{1}{n} \sum_{n=1}^{n_{max}} a_n e^{(\lambda_n t + \phi_n)} f_n(r, t), \tag{2}$$

where $r = \sqrt{x^2 + y^2}$. The background field includes an X-type null point at $x = y = 0$, increases in strength linearly with r and is given by:

$$\psi_0(x, y) \;=\; \frac{1}{2}\left(y^2 - x^2\right)$$

Here lengths have been normalised to the size D of the system (so the outer boundary is at $r = 1$) and field strengths to the value B_0 on the boundary. HOwever, we must use a different set of dimensionless units below to describe particle orbits. The rest of ψ sums over the first n_{max} of the cold plasma eigenmodes originally constructed in Hassam (1992), Craig and McClymont (1991) and Petkaki and MacKinnon (1997) (see also Petkaki (1996)). These eigenmodes have wavelike character far from the null and take on a resistive character at small r. The resistive character is modelled using the plasma resistivity η which is a parameter controlling the size of the diffusion region (Petkaki and MacKinnon, 1997). We include only the azimuthally symmetric eigenmodes that dissipate by reconnection (Craig and McClymont, 1991, 1993; Craig and Watson, 1992).

With randomly chosen phases ϕ_n, a superposition of cold plasma eigenmodes simulates turbulence involving the eigenmodes appropriate to this inhomogeneous situation, taking into account the dissipation that takes place via reconnection at small r (see also McLaughlin, Hood, and De Moortel, 2010). The explicit forms of $\mathbf{B}$ and $\mathbf{E}$ are given in Petkaki and MacKinnon (1997) and are quoted in Appendix B.

The complex eigenvalues λ are written $\lambda = -\kappa + i\omega$;the real numbers ω and κ are frequency and decay rate, respectively. The spatial dependence of the eigenmodes is given by (Hassam, 1992; Petkaki, 1996).

$$f(r) =_2 F_1 \left(-\frac{\kappa}{2} + i\frac{\omega}{2}, \frac{\kappa}{2} - i\frac{\omega}{2}, 1, -\frac{r^2}{\tilde{\eta}\lambda} \right), \tag{3}$$

where $\tilde{\eta}$ is dimensionless resistivity. $_2F_1$ is the Gauss hypergeometric function, the evaluation of which is discussed in Appendix A. Then the eigenvalues λ_n are fixed by the boundary conditions:

$$\Im(f(0)) = 0 \, \Re(f(0) = 1$$

and

$$\Im(f(1)) = 0 = \Re(f(1) = 0$$

Numerically, we found the eigenvalues λ_n using Broyden's method (Press *et al.*, 1992; Petkaki, 1996), using the analytical estimates of Craig and Mc-Clymont (1991) as first guesses. Below we experiment with values of n_{max} up to 49, a large enough number of eigenmodes to produce disordered, noisy fields without excessive computational effort. Eigenfunctions were all normalised to unity at $t = 0$. In the absence of a more detailed model for partition of energy between modes, and to highlight the potential role of turbulence we adopted a flat spectrum, $a_n = 10^{-4}$ for all n.

3 Particle Behaviour: Ions

Here we follow test particles in the presence of our model electric and magnetic fields. Test particle calculations study the behaviour of individual particles while neglecting the self-fields of these same particles. This approach allows us to employ reduced (*e.g.* MHD) descriptions for the electromagnetic fields and, thus, to explore a very large parameter space with reasonable computational effort. The huge disparity of spatial scales involved probably renders a complete description of the plasma impractical for the foreseeable future. This approach allows us to investigate the gross properties that the reconnection must have if it is to actually account for observed particle distributions.

The equations of motion of a charged particle in the presence of a magnetic field are:

$$\frac{d\mathbf{r}}{dt} = \frac{\mathbf{p}}{m\gamma} = \mathbf{v} \tag{4}$$

and

$$\frac{d\mathbf{p}}{dt} = q \left(\mathbf{E} + \frac{1}{c} \left(\mathbf{v} \times \mathbf{B} \right) \right) \tag{5}$$

where $\mathbf{p}$ is the relativistic momentum of a particle, $\mathbf{v}$ is the particle velocity, m is the particle mass, and γ is the Lorentz gamma. A charged particle in a uniform magnetic field where the electric field is equal to zero will travel along a magnetic field line, spiralling around the field line with a gyroradius given by $r_g = \frac{mv_\perp}{|q|B}$. When the gyroradius of the particle becomes comparable to the scale length of the field, the particle will decouple from the field lines, and can gain energy in the presence of an electric field.

3.1   Normalisations

To investigate the motion of particles in our X-type neutral point, it is wise to normalise the problem variables to sensible length and time scales. The equations of motion are normalised in the same manner as the equations of motion in Petkaki and MacKinnon (1997). Specifically, distances are normalised to $d_i = \left(\frac{c^2 m_i}{e B_0} \right)^{1/2}$, where $i = e$ or p for electrons or protons, and $B_0 = B/D$ (the magnetic field at distance D). If we take $B = 100G$ and D to be a typical coronal length scale of 10^9cm then $d_p = 5.6 \times 10^6$cm and $d_e = 1.3 \times 10^5$cm. The velocities then are normalized to the speed of light which is appropriate for the relativistic equations of motion. Our normalising time is derived from these to quantities such that $t_p = 1.87 \times 10^{-4}s$ and $t_e = 4.33 \times 10^{-6}s$. We normalise masses to the particle rest mass. The electric field and the magnetic field are both normalised to $B_0 d_i$.

Although the magnetic field is 2D, the system does have z-translation; hence the particles are allowed to move around in 3D. Equation 6 of Petkaki and MacKinnon (2007) gives the equations of motion of a particle in magnetic and electric fields in 3D for our normalisations. We integrate these numerically, and use our noisy electric and magnetic fields as $\overline{E}$ and $\overline{B}$ (the normalised electric and magnetic fields).

3.2   Particle Energies & Trajectories

To investigate the behaviour of charged particles in our turbulent fields, 10000 ions were released into electric and magnetic fields of the kind shown above, at positions distributed randomly within $0 \leq x \leq 1, 0 \leq y \leq 1$. Their starting energies were chosen randomly from a Maxwellian distribution of temperature $5 \times 10^6 K$, a typical coronal temperature.

3.2.1   Numerics

Since the particle orbits will be integrated numerically, care must be taken to choose a step size that is appropriate to the problem. Smaller step sizes

clearly give more accurate results, but at the expense of longer running times for the simulation. 10000 ions were followed until t=5360 (1s for our normalisations) in constant electric and magnetic fields. The step size was decreased until reducing it further did not alter the distribution of particle energies at t=5360. The largest accurate step size was found to be 0.1, so this was the step size used.

3.2.2 Energy Distributions: Ions

Ions were followed in the presence of five different electric and magnetic fields, composed as follows:

- Case 1: $E = 1 \times 10^{-4}$, $B_x = y$, $B_y = x$. The electric field in this case is constant, and is the same everywhere.

- Case 2: Perturbation for the n=0 mode only. The perturbation has amplitude 1×10^{-4}.

- Case 3: Perturbation for a superposition of modes from n=0 to n=4. Each perturbation has amplitude 1×10^{-4}.

- Case 4: Perturbation for a superposition of modes from n=0 to n=19. Each perturbation has amplitude 1×10^{-4}.

- Case 5: Perturbation for a superposition of modes from n=0 to n=49. Each perturbation has amplitude 1×10^{-4}.

Each mode is also given a random phase at $t = 0$. These phases then remain constant for the rest of the simulation, so that each particle sees the same fields. The resistivity is calculated by considering the time (t_c) a thermal particle takes to cross the non-adiabatic region, *i.e.*:

$$\tilde{\eta} = \frac{1}{4\pi\sigma\tau_p}, \tag{6}$$

where $\sigma = ne^2t/m_e$ and τ_p is our normalising time. By using the time (t) taken for a 1keV proton to travel a distance equal to twice the size of the non-adiabatic region, we can obtain an approximate value for the inertial resistivity (Speiser (1965)). Our dimensionless resistivity is therefore $\tilde{\eta} = 3.1724 \times 10^{-11}$. A sample of the eigenvalues for $\tilde{\eta} = 3.1724 \times 10^{-11}$ (used in calculating the fields) can be seen in Table 1. These decay and oscillation times compare favourably with those in De Moortel, Ireland, and Walsh (2000) (which gives an oscillation time ≈ 180 to ≈ 420s), Aschwanden *et al.* (1999) (which gives an oscillation time ≈ 300s), Verwichte *et al.* (2009) (which

gives an oscillation time 630 ± 30s and a decay time 1000 ± 300s)and De Moortel *et al.* (2002) (oscillation time ≈ 180 to ≈ 300s).

n	Decay time (s) $\left(\frac{1}{\kappa}\right)$	Period(s)$\left(\frac{2\pi}{\omega}\right)$	Frequency(Hz)
0	634.0	244.0	0.0041
1	194.4	77.9	0.0128
2	94.6	46.1	0.0217
3	79.4	32.6	0.0307
4	63.8	25.2	0.0397
5	50.3	20.5	0.0488
10	25.5	10.6	0.0943
15	19.4	7.0	0.1429
20	12.5	5.3	0.1887
25	10.5	4.3	0.2326
30	8.2	3.5	0.2857
35	6.9	3.0	0.3333
40	5.7	2.6	0.3846
45	4.6	2.4	0.4167
49	3.9	2.2	0.4545

Table 1: A selection of values of oscillation time, decay time and period for $\tilde{\eta} = 3.1724 \times 10^{-11}$.

The resulting electric fields are shown in Figure 1. The field for case 2 is almost constant, as the n=0 mode decays very slowly. The field for case 3 actually increases over the time of the simulation. However, this is merely an effect of our choice of end point for the simulation, as higher order modes do oscillate, causing the field to increase and decrease. Over a longer time, the field for case 3 also decays. The fields for cases 4 and 5 appear noisier, although they will also decay over time. The higher order modes will decay first, leaving progressively simpler fields. The particles were followed until t=5360, which is equivalent to 1s if $B_0 = 10^{-7}$. Particles which left the simulation boundary ($x = y = 178, z = 17.8$ in units of d_p) were discarded. These boundaries were chosen to give a system boundary in the x-y plane of 10^9cm (Craig and McClymont (1991)), and a condition that the system width should be around a tenth of its size in the x-y plane (Aschwanden and Nightingale (2005)). These conditions meant that 11 particles from case 3 and 3 particles from case 5 were discarded. The resulting energy distribution is shown in Figure 2.

Figure 2 compares the initial energy distribution of the ions with distributions at t=1s for the static X-type neutral point, for the n=0 mode of
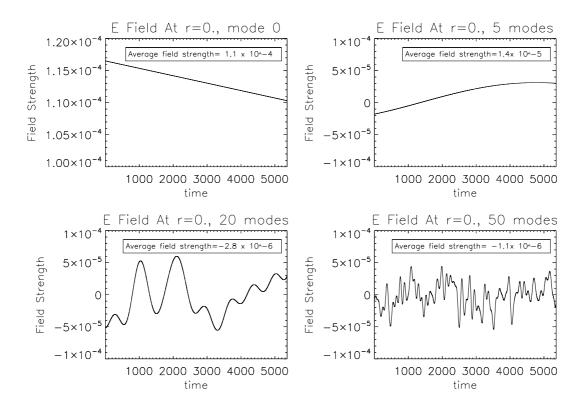
Figure 1: Variation of electric field with time at r=0 with the addition of different numbers of perturbative modes.

oscillation, and for superpositions of 5, 20 and 50 modes. Table 2 shows the percentage of particles which achieved energies above 0.01MeV in each case, along with the peak and mean values of the electric field are $r = 0$ for each case.

Cases 1 and 2 produce similar looking energy distributions, although fewer particles were accelerated to energies above 0.01MeV. In case 1, 3.1% of particles achieved energies above 0.01MeV. In case 2, only 1.6% achieved these energies, although the average electric field strength in these cases is roughly the same. In case 3, 0.3% of particles were accelerated to above 0.01MeV. However the average field strength in this case was also approximately a tenth of that in case 1. Case 4 accelerates 1.2% of particles to above 0.01MeV, around half the number in case 1, but it does so using an average electric field that is almost 40 times smaller than that in case 1. By case 5, a second Maxwellian-type distribution of high energy particles is produced, and 16.9% of particles have energies higher than 0.01MeV. In this case, the average elec-
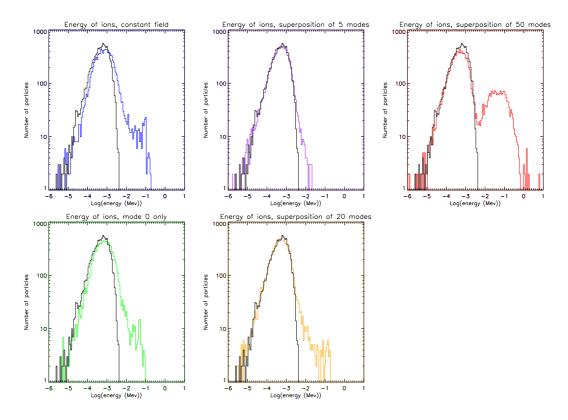
9

Figure 2: Energy distribution of 10000 ions at t=0, and at t=5360 for different electric and magnetic fields.

tric field and the peak amplitude of the electric field are the smallest of any case. The average electric field here is 100 times smaller than that in case 1.

For our normalisations, an electric field of $\overline{E} = 0.0001$ corresponds to an electric field of ≈ 1.8 V/m. Our weakest average electric field (case 5) is therefore ≈ 0.018 V/m, yet it can accelerate particles to energies of almost 1MeV. Dalla and Browning (2005) found that in a 3D static X-type neutral point, electric fields of 1.5kV/m were required to reach these energies (in a system where particles were allowed to move equal distances in x, y and z). The electric field strength in solar flares (Somov, Oreshina, and Kovalenko (2008)) and erupting prominences (Foukal, Little, and Gilliam (1987)) has been measured to be in the region of 1kV/m, around 1000 times larger than the peak value in case 5, which is ≈ 1 V/m. However, solar flare protons with energies in the gigaelectronvolt range, much greater than the energies achieved with this small field, have been observed (*e.g.* Wang and Wang (2006); Kanbach *et al.* (1993); Vilmer *et al.* (2003)). The reconnection electric

Case	Average $|E|$ At $r = 0$	Peak $|E|$ At $r = 0$	% of Protons > 0.01MeV at t=1s
1	$1. \times 10^{-4}$	$1. \times 10^{-4}$	3.1
2	1.1×10^{-4}	1.2×10^{-4}	1.6
3	1.4×10^{-5}	1.9×10^{-4}	0.3
4	2.8×10^{-6}	6.0×10^{-5}	1.2
5	1.1×10^{-6}	5.4×10^{-5}	16.9

Table 2: Number of particles accelerated to above 0.01 MeV with average electric field strength and peak electric field strength in each case.

field has also been observed to be as small as a few hundreds of volts per metre ((Liu and Wang, 2009)). The noisy fields in case 5 seem to be very efficient at accelerating particles. In order to discover the reason behind this acceleration, we must examine a sample of particles in more detail.

3.3   High Energy Particles

In the X-type neutral point model, particles become energised as they pass through the non-adiabatic region around the null, if an electric field is present. We must therefore determine whether particles achieve higher energies for the superpositions of modes because they spend more time in this region, or if there is some other cause. In order to investigate this, the initial positions of all 10000 protons were plotted for each of our simulations.

Figure 3 shows that the size of the region where highly energised particles originate changes as more modes are added. In case 4, we see that high energy particles can originate from a much wider region compared to cases 1 to 3. In case 5, high energy particles can originate from an extended central region, and from a region along the separatrices.

3.4   Determining the Size of the Non-Adiabatic Region

When the motion of the particle is adiabatic, its magnetic moment is conserved. For our normalisations, the magnetic moment is given by (*e.g.* Chen and Torreblanca (1984)):

$$\mu = \frac{v_\perp^2}{|B|} \tag{7}$$

In regions where the magnetic moment of a particle varies, we therefore expect to see a change in the energy of that particle if an electric field is present. Figure 4 shows this relationship. At times and positions where the particle's magnetic moment changes, so does its energy. These large magnetic
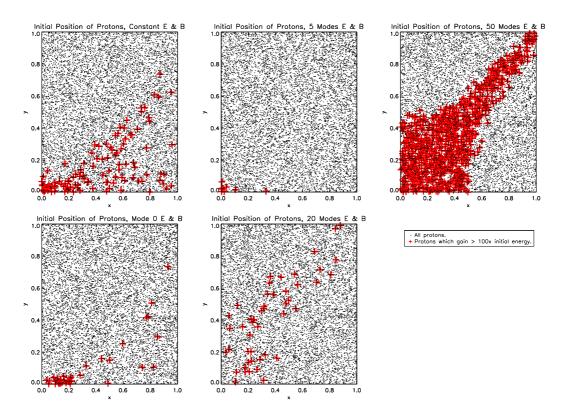
Figure 3: Initial positions of protons for all cases. Dots show the positions (at $t = 0$) of protons energies. Crosses show the positions (at $t = 0$) of protons which gain more than 100 times their d_p.

moment variations occur within $r \approx 0.5$, as do large changes in the particle's energy. This finding is supported by Figure 3, which shows that high energy particles can originate from a central region with radius ≈ 0.5. Compare this with Figure 6, which shows variation in magnetic moment and energy with time and position for case 2. The particles shown do not gain such high energies, and their magnetic moment changes significantly only within $r \approx 0.2$, so any large energy change takes place within a smaller region, meaning that the non-adiabatic region in case 2 is smaller than that in case 5.

Is an increase in the size of the non-adiabatic region solely responsible for the greater energies reached by particles? High energies can also be achieved by multiple crossings of the non-adiabatic region. Figure 5 shows the trajectories in the x-y plane of the two protons shown in Figure 4, as well as the variation of their distance from the neutral point with time. Clearly, the particles spend most of their time orbiting the null at small values of r.
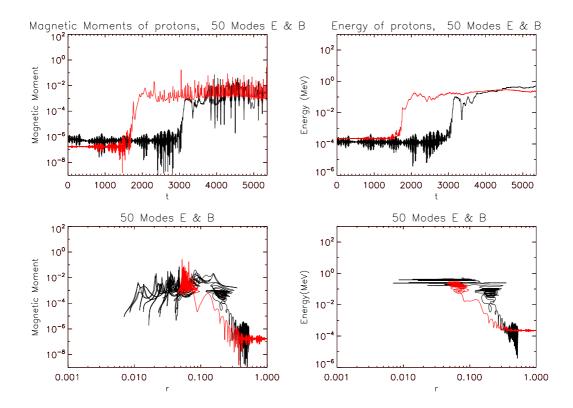
Figure 4: Variation of magnetic moment and energy of high energy particles with distance from the neutral point and time, for case 5. These two particles were chosen as they both gained more than 400 times their original energy. Particle 1 (black) and particle 2 (red) are the same particles in each frame of the figure.

The same plot for case 2 (Figure 7) shows that particles are free to move to large distances from the neutral point when only one eigenmode is present, and that such particles orbit the field lines of a typical-X-point geometry. The two particles shown in Figure 7 move between $r \approx 0.1$ and $r \approx 1$ over the time period of the simulation. The two particles in Figure 4 stay at approximately the same distance from the neutral point for over half the simulation time.

3.5 Magnetic Field Topology

Why do the particles shown in Figure 5 stay so close to the null? Figure 8 shows the shape of the magnetic field close to the null for case 5. For our superposition of modes the centre of the field is significantly altered from a
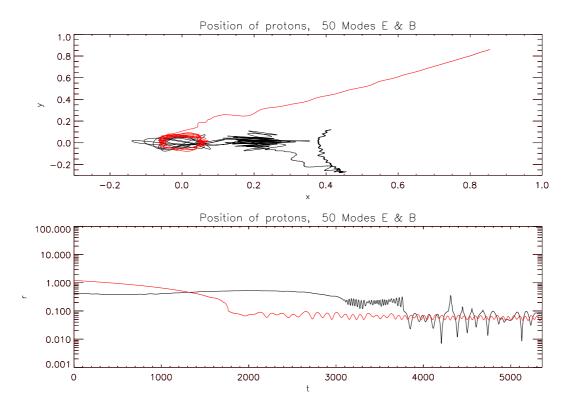
13

Figure 5: Trajectories of two protons in the x-y plane (top) and variation of distance from the neutral point with time (bottom) for case 5. These two particles were chosen as they both gained more than 400 times their original energy. Particle 1 (black) and particle 2 (red) are the same particles in each frame of the figure.

standard X-type neutral point. The field for case 5 contains a region of closed magnetic field (an O-type neutral point) at its centre where the particle can become trapped. Since these closed regions are within $r \approx 0.5$, where we have seen the particles can move non-adiabatically, particles which become trapped in these regions can gain significant amounts of energy. The trajectory of one such particle is shown; the particle is seen to be approximately following one of the central circular field lines. Note that the field is plotted at $t = 0.5s$, but the trajectory shown is the path taken by the proton over the whole time of the simulation. However, the central loop that the particle is following remains approximately constant in size and shape throughout the simulation. Near the null, we also see the development of many smaller X-type and O-type points, which will also be regions of particle demagneti-
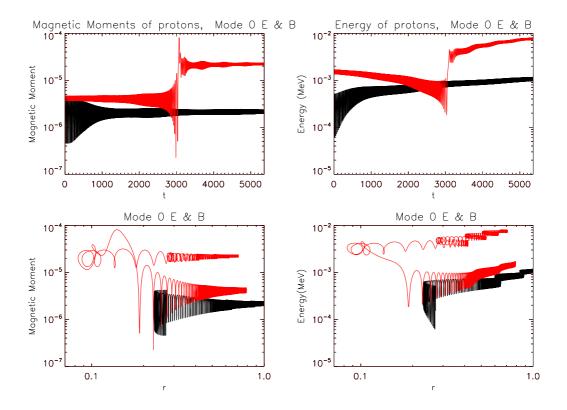
14

Figure 6: Variation of magnetic moment and energy of high energy particles with distance from the neutral point and time, for case 2.These two particles were chosen as they both gained more than 5 times their original energy. Particle 1 (black) and particle 2 (red) are the same particles in each frame of the figure.

sation, and therefore give rise to acceleration in the presence of an electric field. Such magnetic structures are reminiscent of those caused by a tearing mode instability when a plasma with finite conductivity (such as the plasma we simulate) is perturbed at an X-type point(Furth, Killeen, and Rosenbluth (1963)).

4   Summary and Conclusion

In this work we have investigated the consequences for the acceleration of protons by reconnection at a steady X-type neutral point and in noisy electric and magnetic fields. In future work we intend to look at the acceleration of thermal electrons in similarly turbulent reconnection situations. This work
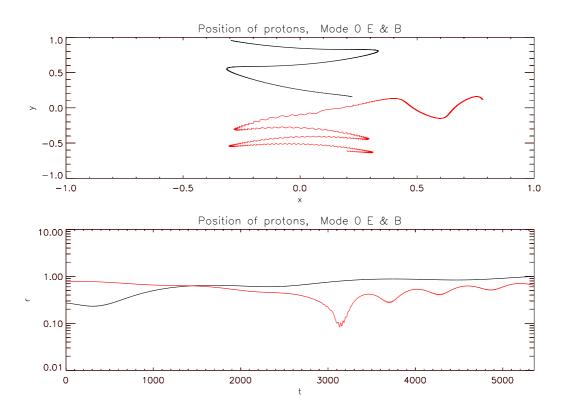
15

Figure 7: Trajectories of two protons in the x-y plane (top) and variation of distance from the neutral point with time (bottom) for case 2. These two particles were chosen as they both gained more than five times their original energy. Particle 1 (black) and particle 2 (red) are the same particles in each frame of the figure

follows particles in the presence of a 2D magnetic field. A third component B_z of the equilibrium field would modify the structure of E and B, but Hamilton *et al.* (2005) show that a regime of sufficiently small B_z exists in which the resulting modifications are negligible for particle acceleration purposes. Larger B_z would result in reduced reconnection rate (and thus electric fields) and would introduce time-dependent structure in the z direction, a more complex situation which we do not investigate here. The addition of a non-zero B_z component merely increases the efficiency of the acceleration, as particles tend to stay within the current sheet (see also Litvinenko (1996)). This means that the energies gained by particles in our simulations are likely to be at the lower end of the energy range that could be achieved with a 3D geometry. Future work will explore the consequences of a 3D geometry for

16

our simulations.

Various physical effects would result from relaxing our 2D, cold plasma model. Gruszecki *et al.* (2011) show that nonlinear effects become important as waves propagate towards the null, at a distance determined by plasma beta and the amplitude of the disturbance. Departures from azimuthal symmetry occur along with localised current spikes, all of which would have implications for accelerated particles. The plasma beta here is identically zero, which minimises these effects, although they could become important in a more realistic treatment.

The eigenmode solutions are mathematically valid for any value of the scalar resistivity. In Section 3.2.2 we estimated a value of inertial resistivity roughly two orders of magnitude greater than the Spitzer value (which is 2.2×10^{-13} in our dimensionless units). If only Spitzer resistivity is applied the size of the central diffusion region (which is $O(\eta^{1/2})$ (Craig and McClymont (1991))), would be roughly one order of magnitude smaller. However the character of the solution in the outer, advection region depends only weakly on η. While the detailed locations change, the secondary O- and X-type nulls shown in Figure 8 still exist to provide particle acceleration through a large volume. In practice enhanced resistivity might also result from other factors (*e.g.* ion-acoustic resistivity, Petkaki and Freeman (2008))

Superpositions of eigenmode oscillations of standing waves were used to produce noisy electric and magnetic fields appropriate to the background geometry. At an X-type neutral point, particles generally gain energy in the region around the null where the magnetic field falls to zero. However, in the presence of a noisy electromagnetic field superimposed onto the X-type neutral point magnetic field, protons could be accelerated to relativistic energies, producing a high energy 'tail'. This acceleration is due to the creation of a larger central non-adiabatic region, as evidenced by the change in magnetic moment at greater distances from the neutral point when more oscillations are added to the electric and magnetic fields. The increase in the area from which high energy particles can originate is further evidence for a larger non-adiabatic region. In addition, adding more perturbative modes to the electric and magnetic fields causes the shape of the magnetic field to be altered. The change in the magnetic field structure produces more null points near the centre of the field, and also creates regions of closed magnetic field where particles can become trapped and gain substantial amounts of energy.

These results may provide insight into flare ion acceleration in two ways. First, they show how the inclusion of physically realistic 'noise' around a reconnection region allows higher particle energies to be attained, approaching the γ-ray emitting energy range. Second, they show how turbulence also allows particles to be accelerated through a larger region, increasing the

17

total number of particles accelerated. The extent to which these processes can bring reconnection region particle acceleration closer to observational constraints will be investigated in future work.

Acknowledgements

A   The Hypergeometric Function

$_2F_1(a, b; c; z)$ is given by (Abramowitz and Stegun (1965), Chapter 15):

$$_2F_1(a, b; c; z) = \sum_{i=0}^{n} \frac{(a)_n (b)_n}{(c)_n} \frac{z^n}{n!}, \tag{8}$$

where $(x)_n = x(x+1)(x+2)...(x+n-1)$. Equation (8) converges only for $|z| < 1$. An efficient evaluation for $|z| > 1$ is achieved via a transformation formula (Abramowitz and Stegun (1965)):

$$_2F_1(a, b; c; z) = \frac{\Gamma(c)\Gamma(b-a)}{\Gamma(b)\Gamma(c-a)}(-z)^{-a}{}_2F_1(a, 1-c+a; 1-b+a; \frac{1}{z})$$

$$+ \frac{\Gamma(c)\Gamma(a-b)}{\Gamma(a)\Gamma(c-b)}(-z)^{-b}{}_2F_1(b, 1-c+b; 1-a+b; \frac{1}{z}). \tag{9}$$

For the calculation of the magnetic field perturbation, the derivative of the hypergeometric function is used, which is given by Abramowitz and Stegun (1965) as:

$$\frac{d}{dz}F(a, b; c; z) = \frac{ab}{c}F(a+1, b+1; c+1; z).$$

B Explicit Forms of Electric and Magnetic Fields

The electric fields we use are the same as those given in Petkaki and MacKinnon (1997).

$$\overline{E_z} = A_0[exp(-\kappa t)[\kappa(cos(\omega t)f_\Re sin(\omega t)f_\Im) + \omega(cos(\omega t)f_\Im + sin(\omega t)f_\Re)]], \tag{10}$$

$$\overline{B_x} = \overline{y}[1 + A_0\frac{1}{2\eta}exp(-\kappa t)[\kappa(cos(\omega t)f'_\Re - sin(\omega t)f'_\Im) + \omega(sin(\omega t)f'_\Re + cos(\omega t)f'_\Im)]], \tag{11}$$

$$\overline{B_y} = \overline{x}[1 - A_0\frac{1}{2\eta}exp(-\kappa t)[\kappa(cos(\omega t)f'_\Re - sin(\omega t)f'_\Im) + \omega(sin(\omega t)f'_\Re + cos(\omega t)f'_\Im)]]. \tag{12}$$

A_0 is the amplitude of the fluctuation, which we have chosen to be 1×10^{-4} for all modes. η is the resistivity, f is the hypergeometric function and f' is its derivative. Bars denote quantities which are in our dimensionless units.

References

Abramowitz, M., Stegun, I.A.: 1965, *Handbook of mathematical functions with formulas, graphs, and mathematical tables.*

Aschwanden, M.J., Nightingale, R.W.: 2005, Elementary Loop Structures in the Solar Corona Analyzed from TRACE Triple-Filter Images. *Astrophys. J.* **633**, 499 – 517. doi:10.1086/452630.

Aschwanden, M.J., Fletcher, L., Schrijver, C.J., Alexander, D.: 1999, Coronal Loop Oscillations Observed with the Transition Region and Coronal Explorer. *Astrophys. J.* **520**, 880 – 894. doi:10.1086/307502.

Bulanov, S.V., Syrovatskii, S.I.: 1980, MHD oscillations and waves near a magnetic null line. *Soviet Journal of Plasma Physics* **6**, 1205 – 1218.

Chen, F.F., Torreblanca, H.: 1984, *Introduction to plasma physics and controlled fusion, 2nd edition.*

Craig, I.J., Watson, P.G.: 1992, Fast dynamic reconnection at X-type neutral points. *ApJ* **393**, 385 – 395. doi:10.1086/171512.

Craig, I.J.D., McClymont, A.N.: 1991, Dynamic magnetic reconnection at an X-type neutral point. *ApJ Letters* **371**, L41 – L44. doi:10.1086/185997.

Craig, I.J.D., McClymont, A.N.: 1993, Linear theory of fast reconnection at an X-type neutral point. *ApJ* **405**, 207 – 215. doi:10.1086/172354.

Dalla, S., Browning, P.K.: 2005, Particle acceleration at a three-dimensional reconnection site in the solar corona. *Astron. Astrophys.* **436**, 1103 – 1111. doi:10.1051/0004-6361:20042589.

De Moortel, I., Ireland, J., Walsh, R.W.: 2000, Observation of oscillations in coronal loops. *Astron. Astrophys.* **355**, L23 – L26.

De Moortel, I., Ireland, J., Hood, A.W., Walsh, R.W.: 2002, The detection of 3 & 5 min period oscillations in coronal loops. *Astron. Astrophys.* **387**, L13 – L16. doi:10.1051/0004-6361:20020436.

Foukal, P., Little, R., Gilliam, L.: 1987, Paschen-line Stark-broadening as an electric field diagnostic in erupting prominences. *Solar Phys.* **114**, 65 – 73.

Furth, H.P., Killeen, J., Rosenbluth, M.N.: 1963, Finite-Resistivity Instabilities of a Sheet Pinch. *Phys. Fluids* **6**, 459 – 484. doi:10.1063/1.1706761.

Gruszecki, M., Vasheghani Farahani, S., Nakariakov, V.M., Arber, T.D.: 2011, Magnetoacoustic shock formation near a magnetic null point. *Astron. Astrophys.* **531**, A63. doi:10.1051/0004-6361/201116753.

Guo, J.-N., Büchner, J., Otto, A., Santos, J., Marsch, E., Gan, W.-Q.: 2010, Is the 3-D magnetic null point with a convective electric field an efficient particle accelerator? *Astron. Astrophys.* **513**, A73. doi:10.1051/0004-6361/200913321.

Hamilton, B., Fletcher, L., McClements, K.G., Thyagaraja, A.: 2005, Electron Acceleration at Reconnecting X-Points in Solar Flares. *Astrophys. J.* **625**, 496 – 505. doi:10.1086/430100.

Hassam, A.B.: 1992, Reconnection of stressed magnetic fields. *ApJ* **399**, 159 – 163. doi:10.1086/171911.

Kanbach, G., Bertsch, D.L., Fichtel, C.E., Hartman, R.C., Hunter, S.D., Kniffen, D.A., Kwok, P.W., Lin, Y.C., Mattox, J.R., Mayer-Hasselwander, H.A.: 1993, Detection of a long-duration solar gamma-ray flare on June 11, 1991 with EGRET on COMPTON-GRO. *Astron. Astrophys. Suppl.* **97**, 349 – 353.

Lin, R.P., Krucker, S., Hurford, G.J., Smith, D.M., Hudson, H.S., Holman, G.D., Schwartz, R.A., Dennis, B.R., Share, G.H., Murphy, R.J., Emslie,

A.G., Johns-Krull, C., Vilmer, N.: 2003, RHESSI Observations of Particle Acceleration and Energy Release in an Intense Solar Gamma-Ray Line Flare. *Astrophys. J. Lett.* **595**, L69 – L76. doi:10.1086/378932.

Litvinenko, Y.E.: 1996, Particle Acceleration in Reconnecting Current Sheets with a Nonzero Magnetic Field. *Astrophys. J.* **462**, 997. doi:10.1086/177213.

Litvinenko, Y.E.: 2003, Particle Acceleration by a Time-Varying Electric Field in Merging Magnetic Fields. *Solar Phys.* **216**, 189 – 203. doi:10.1023/A:1026143310271.

Liu, C., Wang, H.: 2009, Reconnection Electric Field and Hardness of X-Ray Emission of Solar Flares. *Astrophys. J. Lett.* **696**, L27 – L31. doi:10.1088/0004-637X/696/1/L27.

McLaughlin, J., Hood, A., De Moortel, I.: 2010, Review article: Mhd wave propagation near coronal null points of magnetic fields. *Space Sci. Rev.*, 1 – 32. 10.1007/s11214-010-9654-y. http://dx.doi.org/10.1007/s11214-010-9654-y.

Parker, E.N.: 1963, The Solar-Flare Phenomenon and the Theory of Reconnection and Annihiliation of Magnetic Fields. *ApJ* **8**, 177 – +. doi:10.1086/190087.

Petkaki, P.: 1996,. PhD thesis, University of Glasgow.

Petkaki, P., Freeman, M.P.: 2008, Nonlinear Dependence of Anomalous Ion-Acoustic Resistivity on Electron Drift Velocity. *Astrophys. J.* **686**, 686 – 693. doi:10.1086/590654.

Petkaki, P., MacKinnon, A.L.: 1997, Particle Acceleration in Dynamical Collisionless Reconnection. *Sol.Phys.* **172**, 279 – 286.

Petkaki, P., MacKinnon, A.L.: 2007, Particle acceleration by fluctuating electric fields at a magnetic field null point. *Astron. Astrophys.* **472**, 623 – 632.

Petkaki, P., MacKinnon, A.L.: 2011, Acceleration of charged particles by fluctuating and steady electric fields in a X-type magnetic field. *Advances in Space Research* **48**, 884 – 898. doi:10.1016/j.asr.2011.04.019.

Petschek, H.E.: 1964, Magnetic Field Annihilation. *NASA Special Publication* **50**, 425 – +.

Press, W.H., Teukolsky, S.A., Vetterling, W.T., Flannery, B.P.: 1992, *Numerical recipes in FORTRAN. The art of scientific computing.*

Priest, E., Forbes, T.: 2000, *Magnetic Reconnection.*

Somov, B.V., Oreshina, I.V., Kovalenko, I.A.: 2008, Magnetic reconnection, electric field, and particle acceleration in the July 14, 2000 solar flare. *Astronomy Letters* **34**, 327 – 336. doi:10.1134/S1063773708050058.

Speiser, T.W.: 1965, Particle Trajectories in Model Current Sheets, 1, Analytical Solutions. *J. Geophys. Res.* **70**, 4219 – 4226. doi:10.1029/JZ070i017p04219.

Sweet, P.A.: 1958, The Neutral Point Theory of Solar Flares. In: B. Lehnert (ed.) *Electromagnetic Phenomena in Cosmical Physics*, IAU Symposium **6**, 123 – +.

Verwichte, E., Aschwanden, M.J., Van Doorsselaere, T., Foullon, C., Nakariakov, V.M.: 2009, Seismology of a large solar coronal loop from euvi/stereo observations of its transverse oscillation. *Astrophys. J.* **698**, 397 – 404. doi:10.1088/0004-637X/698/1/397.

Vilmer, N., MacKinnon, A.L., Trottet, G., Barat, C.: 2003, High energy particles accelerated during the large solar flare of 1990 May 24: X/γ-ray observations. *Astron. Astrophys.* **412**, 865 – 874. doi:10.1051/0004-6361:20031488.

Wang, R., Wang, J.: 2006, Spectra and solar energetic protons over 20 GeV in Bastille Day event. *Astroparticle Physics* **25**, 41 – 46. doi:10.1016/j.astropartphys.2005.11.002.

White, S.M., Benz, A.O., Christe, S., Fárnik, F., Kundu, M.R., Mann, G., Ning, Z., Raulin, J.-P., Silva-Válio, A.V.R., Saint-Hilaire, P., Vilmer, N., Warmuth, A.: 2011, The Relationship Between Solar Radio and Hard X-ray Emission. *Space Sci. Rev.* **159**, 225 – 261. doi:10.1007/s11214-010-9708-1.
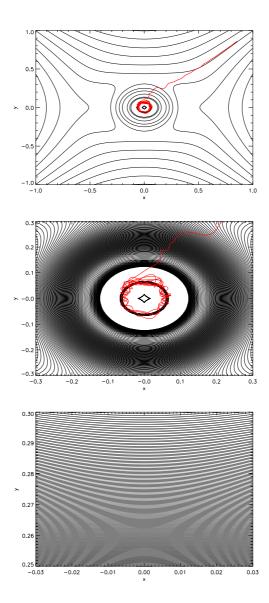
Figure 8: Magnetic field contours with a sample particle trajectory over-plotted for case 5, for the region $-1 \leq x \leq 1$, $-1 \leq y \leq 1$ (top), for the region $-0.3 \leq x \leq 0.3$, $-0.3 \leq y \leq 0.3$ (middle), and for the region $-0.03 \leq x \leq 0.03$, $0.25 \leq y \leq 0.3$ (bottom), displaying some of the smaller nulls formed by the perturbations. Note that the field is plotted at $t = 0.5s$, but the trajectory shown is the path taken by the proton over the entire simulation time. However, the central loop that the particle is following remains approximately constant in size and shape throughout the simulation.